Evolution of the Plasma Universe: II. The Formation of Systems of Galaxies

ANTHONY L. PERATT, SENIOR MEMBER, IEEE

Abstract—**The model of the plasma universe, inspired by totally unexpected phenomena observed with the advent and application of fully three-dimensional electromagnetic particle-in-cell simulations to filamentary plasmas, consists of studying the interaction between field-aligned current-conducting, galactic-dimensioned plasma sheets or filaments (Birkeland currents). In a preceding paper, the evolution of the interaction spanned some 10^8–10^9 years, where simulational analogs of synchrotron-emitting double radio galaxies and quasars were discovered. This paper reports the evolution through the next 10^9–5×10^9 years. In particular, reconfiguration and compression of tenuous cosmic plasma due to the self-consistent magnetic fields from currents conducted through the filaments leads to the formation of elliptical, peculiar, and barred and normal spiral galaxies. The importance of the electromagnetic pinch in producing condense states and initiating gravitational collapse of dusty galactic plasma to stellisimals, then stars, is discussed. Simulation data are directly compared to galaxy morphology types, synchrotron flux, HI distributions, and fine detail structure in rotational velocity curves. These comparisons suggest that knowledge obtained from laboratory, simulation, and magnetospheric plasmas offers not only to enhance our understanding of the universe, but also to provide feedback information to laboratory plasma experiments from the unprecedented source of plasma data provided by the plasma universe.**

I. Introduction

THE evolution of cosmic plasma from a filamentary state to the development of double radio sources and quasars was investigated in the first part to this sequel paper (Paper I) [1]. The time frame of this study, based upon scaling simulation parameters to galactic dimensions, spanned some 10^8–10^9 years. In this paper (Paper II), the evolution for the next 1–5×10^9 years under the influence of electromagnetic forces acting on the plasma is investigated.

The importance of electromagnetic forces in galactic and stellar evolution derives from the fact that the universe is largely matter in its plasma state. The observed stars are composed of plasmas, as are the interstellar and interplanetary media and the outer atmospheres of planets. The neutral HI regions in galaxies are also plasma although the degree of ionization is probably only 10^{-4}. Both the intra- and intergalactic media then consist of plasma, leading to the coinage of the term "plasma universe." Electromagnetic forces can then be expected to play a crucial role in the development of the plasma universe including both the formation of systems of galaxies and the formation of stars within the dusty galactic plasmas [2]–[4].

Although the gravitational force is weaker than the electromagnetic force by 39 orders of magnitude, gravitation is one of the dominant forces in astrophysics when electromagnetic forces neutralize each other, as is the case when large bodies form [5]. Indicative of the analogy of forces for the motion of electrons and ions in the electromagnetic field and the motion of large bodies in the gravitational field is the ease with which a plasma model may be changed to a gravitational model. This transformation requires only a change of sign in the (electrostatic) potential calculation such that like particles attract instead of repel, followed by setting the charge-to-mass ratio equal to the square root of the gravitational constant (a gravitational model cannot be simply changed to an electromagnetic model as the full set of Maxwell's equations are required in the latter).

The basic model of the plasma universe, inspired by the observation that most cosmic plasmas are filamentary in structure [6], consists of studying the interaction between current-conducting galactic-dimensioned plasma filaments aligned along magnetic field lines (Birkeland currents, [1]). Although the entire filamental circuit is expected to be hundreds of megaparsecs in length and is probably no less complex than the magnetospheric current distribution near Earth, only a fraction of the circuit is simulated. The fraction of the length corresponds to a local region that is capable of interacting with an adjacent local region in a neighboring filament. Strictly speaking, the neighboring regions in adjacent filaments are double layers since the model consists of a parallel electric field in each of the pinched plasma filaments [7]. Because of the axial E field, electrons within the pinch are accelerated along the filament producing strong currents and also radiating away energy in the form of synchrotron radiation at radio, optical, and X-ray wavelengths.

It is the purpose of this paper to continue the investigation of the dynamics of the denser interacting plasmas pinched within the filaments by means of the electromagnetic and gravitational force laws. That this is possible is due largely to the advent of the particle simulation of dynamic systems in three dimensions on large computers, allowing the computation of up to many millions of charge and mass particles according to their respective force laws. This approach to the study of cosmic plasma is labeled "gravito-electrodynamic" [8].

Manuscript received June 6, 1986; revised July 17, 1986.

The author is with the Los Alamos National Laboratory, Los Alamos, NM 87545.

IEEE Log Number 8610914.

0093-3813/86/1200-0763$01.00 © 1986 IEEE

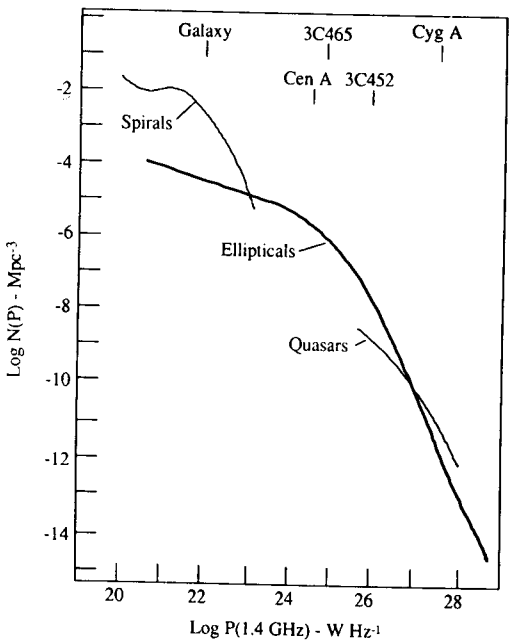

Fig. 1. The radio luminosity function of galaxies and quasars at the present cosmological epoch (adapted from Fanti and Perola [10]).

The gross radio properties of galaxies are reviewed in Section II. Section III describes a transistion through the following sequence of cosmic objects: double radio galaxy to radioquasar; radioquasar to radioquiet quasi-stellar objects (QSO's) [9]; radioquiet QSO's to peculiar and Seyfert spiral galaxies; and peculiar and Seyfert galaxies to normal and barred galaxies. The various classifications of elliptical and spiral galaxies are discussed in Sections IV and V, respectively. The importance of electromagnetic effects in describing both the bulk- and fine-detail structure in the velocity curves of spiral galaxies is also reported in Section V. Multiple interacting galaxies are studied in Section VI. The chemical composition and the distribution of neutral hydrogen in galaxies is discussed in Section VII. Section VIII covers the Alfvén–Carlqvist model for star formation in pinched plasma filaments while Section IX reports the extension of three-dimensional electromagnetic particle simulation techniques to include gravitational forces with the formation of stars.

II. Gross Radio Properties of Galaxies

The radio power L of galaxies, integrated from 10 MHz to 100 GHz, ranges from about 10^{30} to about 10^{38} W, and relative to their optical luminosity from less than 10^{-6} to about 1 [10], [11]. The distribution in power is described by means of the radio luminosity function (RLF), which represents the number of radio-emitting galaxies per unit volume as a function of the monochromatic power at a certain frequency. Fig. 1 illustrates the RLF at 1.4 GHz at the present cosmological epoch, the "local" RLF.

The RLF suggests a continuity in the morphological types of radio-emitting galaxies. Above 10^{26} W/Hz, the main contribution comes from quasars and classical double radio galaxies. In the region 10^{23}–10^{26} W/Hz, the elliptical galaxies dominate, while below 10^{23} W/Hz (about an order of magnitude greater than the power of our Galaxy) the power comes principally from spiral galaxies.

TABLE I
Properties of Synchrotron-Emitting Galactic Radio Sources

Source	Power, W/Hz	Geometry and Dimension	Red-Shift, z
double radio galaxies, quasars	10^{26}-10^{29}	two extended radio lobes separated tens of Kpc to tens of Mpc; oftentimes a central component is present	0.01-1.8 0.3-3.8
ellipticals	10^{23}-10^{26}	kiloparsecs to decaparsecs	
cD		giant ellipticals with very extended haloes	~1
N		bright nucleus surrounded by faint nebulosity	
	$10^{24.5}$	break in RLF	
	10^{26}	Seyfert-like spectra	
Seyfert spirals		elementary spirals of a few tens of kpc extent; most active nuclei.	0.02-0.09
spirals	$<10^{23}$	two radio components: ~10Kpc coincident with spiral disk, ≤Kpc nuclear region.	0.003-0.5 (Andromeda is blue-shifted)
	$10^{21.3}$	break in RLF	

In the region 10^{21}–10^{23} W/Hz, an overlap of spiral and elliptical galaxies occurs. The "ellipticals" are in fact a hybrid class, containing bona fide ellipticals along with N galaxies (a bright nucleus surrounded by a faint nebulosity) to that of cD galaxies (giant ellipticals with very extended radio "halos"). Noteworthy in Fig. 1 is a "break" in synchrotron power from ellipticals at $10^{24.5}$ W/Hz and another at $10^{21.3}$ W/Hz for spirals.

The size of the radio-emitting regions in galaxies spans a very wide range. At powers larger than about 10^{23} W/Hz at 1.4 GHz the radio emission is generally dominated by an extended component, whose size goes from tens of kiloparsecs (e.g., Cyg A) to tens of megaparsecs (e.g., 3C236). Often a very compact central radio component is present, whose power ranges from 10^{22} up to 10^{25} W/Hz, and which may be seen to vary with time. Extended and central radio components are typically found also in quasars.

At powers less than about 10^{23} W/Hz the size of the radio region in elliptical galaxies is generally measured in kiloparsecs and often reduces to a compact central component. In spiral galaxies, the next stage of a suggested epochological sequence in Fig. 1, the situation is different. Apart from the radical change in morphology between elliptical and spiral, the spiral galaxies have not only a compact nuclear component (of radio dimension between 0.1 and 1 kpc) but also a component of size ~ 10 kpc coincident with the spiral disk.

Overlapping the powerful radio ellipticals having Seyfert-like nuclear spectra and the spiral galaxies are the Seyfert spirals themselves, comprising 1 percent of all spiral types. In contrast to the ellipticals, spiral galaxies rarely have compact nuclear sources and are rarely associated with extended radio lobes. Table I delineates the properties of galactic radio sources with decreasing redshift.

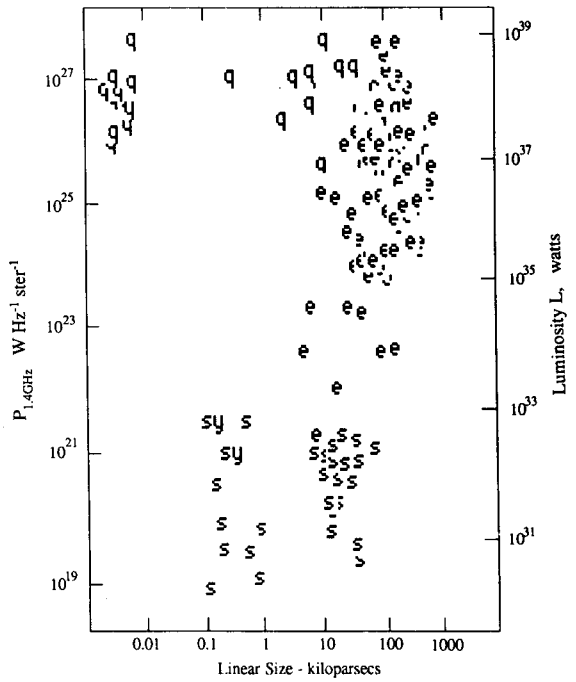

Fig. 2. Plot of the monochromatic radio power at 1.4 GHz versus linear diameter for classes of extragalactic radio sources. The symbol *e* denotes extended radio sources associated with elliptical galaxies while *q* and *s* denote quasars and spiral galaxies, respectively (adapted from Eckers [12]).

Fig. 2 shows the positions of the radio sources, both extended and compact on a linear-size radio-luminosity plot [12]. As seen, the bulk of the classical double radio galaxies possessing an elliptical galaxy have a spatial extent between a few tens of kiloparsecs to many hundreds of kiloparsecs, with radio luminosities of $L \sim 10^{35}$–10^{39} W. Some transitional radio galaxies, 8–80 kpc, $L \sim 10^{34}$ W, are also present. The radioquasars appear in two distinct populations; extended sources with dimensions of several kiloparsecs to several hundreds of kiloparsecs ($L \sim 10^{37}$–10^{39} W), and compact sources ~2–8 pc ($L \sim 10^{37}$–10^{39} W). Most of the spiral galaxies are found to be clustered according to a size-luminosity of ~10–80 kpc, $L \sim 10^{31}$–$10^{32.5}$ W.

Finally, unlike the other properties, the radio spectra of the spiral galaxies are similar to those of the radio galaxies. The remainder of this paper addresses the evolutionary sequence suggested by the data above.

III. The Transition from Double Radio Galaxies to Spiral Galaxies

The transition of two interacting Birkeland currents of galactic dimensions [1] into the morphology of a spiral galaxy is best seen in time-lapse photography (16-mm films) from the long-time simulation runs. The reason for this is the rapidity with which the spiral is formed once the distance between interacting plasmas has closed to the order of a filament radii. Nevertheless, single frame photographs from the simulations can perhaps convey the gross morphological change (but do not convey the dynamics of the plasma within the bulk forms). These are shown in Figs. 3–7.

Figs. 4, 5, and 6 pertain to the cross-sectional views of two plasma filaments (the "extended components") of width ~35 kpc and separation ~80 kpc. (The axial extent is determined either by the length of the "micropinch" within the filament (in comparison to the analogy of laboratory filaments) or to the width of the double layer formed in the Birkeland current; these are typically comparable to the filamental width). Fig. 5 ($\omega_c/\omega_p = 3$) has an axial magnetic field strength twice that of Fig. 4 ($\omega_c/\omega_p = 1.5$). Fig. 6 pertains to $\omega_c/\omega_p = 3.0$, and an initial thermal plasma of 32 KeV. Fig. 7 compares selected simulation frames of a single simulation run to three galaxy morphological types.

The transition proceeds as follows. For the case of a field-aligned electric field $\boldsymbol{E} \| \boldsymbol{B}$, oriented along the $+z$ direction (out of the plane of the figure) in the columns, the electrons in both columns spiral downward in counterclockwise rotation. Likewise, the ions spiral upward in clockwise rotation. The current density is $\boldsymbol{j} = n_e q_e \upsilon_e + n_i q_i \upsilon_i$ where the subscripts e and i denote electrons and ions, respectively. The quantity q is the charge on the particle, $n_e = n_i$ and $|\upsilon_e| >> |\upsilon_i|$ are the average (drift) velocities. For the initial separations depicted in the first few frames of Figs. 4–6, the Biot–Savart force is predominantly attractive [1, sec. IV] and the relative velocity of the two plasma filaments are approximately 1000 km/s ($T \approx 100$, [1, sec. VI-B]).

The relative velocity of the plasmas increases directly with increasing current and reaches a velocity of several thousand kilometers per second near minimum separation ($T \approx 400$, Fig. 5). The simulation current ranges from about 2×10^{19} to 4×10^{20} A in Fig. 5. Collision does not occur because the repulsive force of the counterparallel azimuthal currents becomes equal to, then exceeds, the attractive force at separations of the order of the plasma radii. At this time the translational momentum is converted into angular momentum because of the $\tau = \boldsymbol{m} \times \boldsymbol{B}$ torque between filaments (left-hand or clockwise twist) where $\boldsymbol{m}$ is the magnetic moment of a filament. Concomitant with the attraction, repulsion, and rotation, is a reconfiguration of the current/plasma cross-sectional profiles in the filaments. In particular, the initially circular cross sections are deformed into oval shapes that then take on a "jelly-bean-like" profile prior to forming embryonic spiral arms. During this process, the elliptically shaped quasar formed midway between the two synchrotron radiating plasmas is enclosed by the plasmas themselves, as they spiral inward. During this time, the quasar dimensions narrow and the enclosed sump density increases because of the increasing isobaric pressure. The ~50-kpc channel ($T \approx 255$) is reduced to a few kiloparsecs length [1, fig. 12]. The trailing spiral arms then lengthen with time. Bostick [13], [14] was the first to record the formation of spiral structures in the laboratory from interacting plasmoids and to note the striking similarity to their galactic analogs.

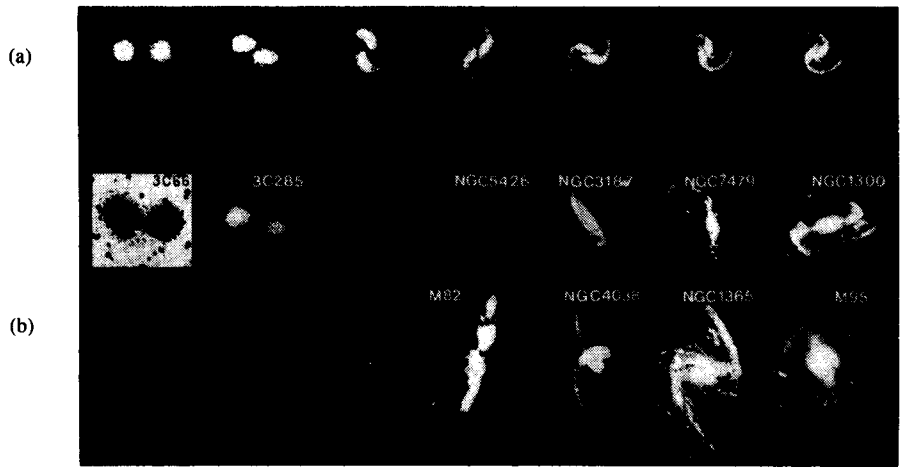

Fig. 3. (a) Single-frame stills of plasma in galaxy simulation run DD4. $\omega_c/\omega_p = 3.0$, $T_{e0} = T_{i0} = 32$ keV, $T = 1$–1300. (b) Optical photographs of selected galaxies.

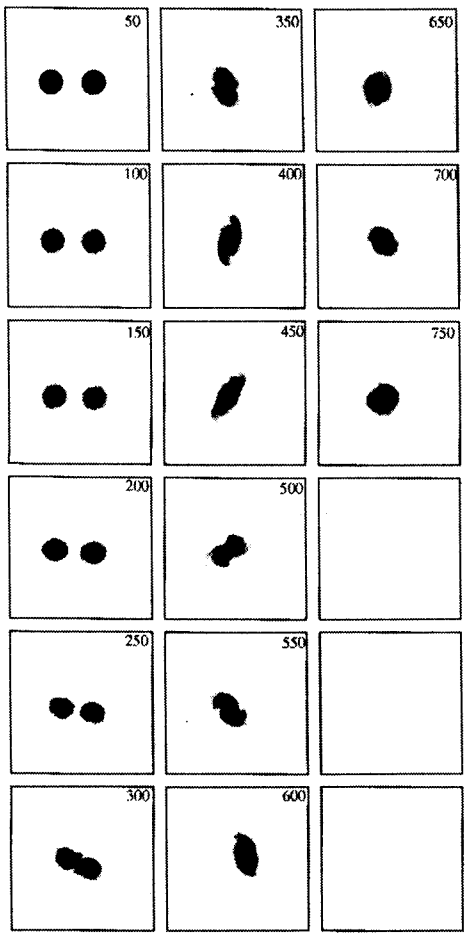

Fig. 4. Single-frame stills of plasma in galaxy simulation T06. $\omega_c/\omega_p = 1.5$, $T_{e0} = T_{i0} = 2$ keV, $T = 1$–750. Acceleration field, 0.002 cells per time step squared. Not shown is the intergalactic plasma trapped at the geometric center.

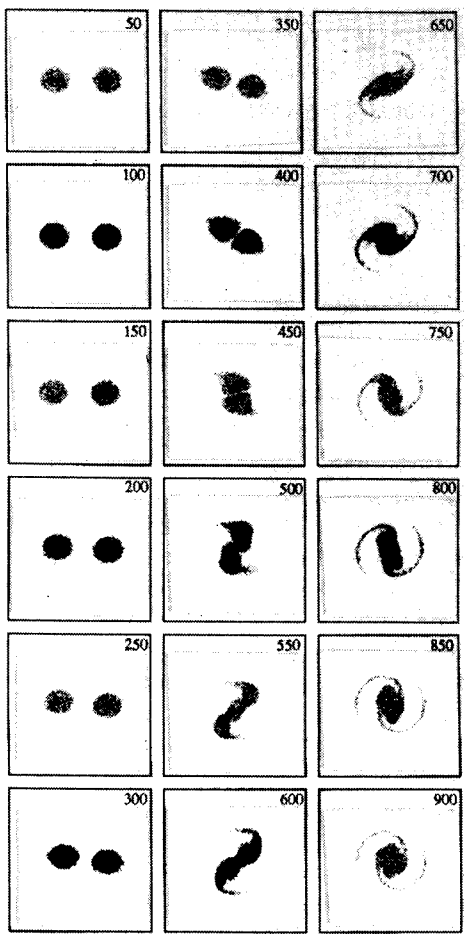

Fig. 5. Single-frame stills of plasma in galaxy simulation run T6B. $\omega_c/\omega_p = 3.0$, $T_{e0} = T_{i0} = 2$ keV, $T = 1$–900. Acceleration field, 0.002 cells per time step squared. Not shown is the intergalactic plasma trapped at the geometric center.

A. Double Radio Galaxy to Radioquasar

In Paper I the formation of a double radio galaxy and its transition to a radioquasar were investigated. Comparison of Fig. 4 and Fig. 8 [1, fig. 15, probe 4] delineates the following sequence of events:

1) the condensation of current-carrying plasma into the two pinched filaments, $T \approx 20$–50;
2) formation of an elliptical sump midway between filaments with subsequent capture and compression of intergalactic plasma; and

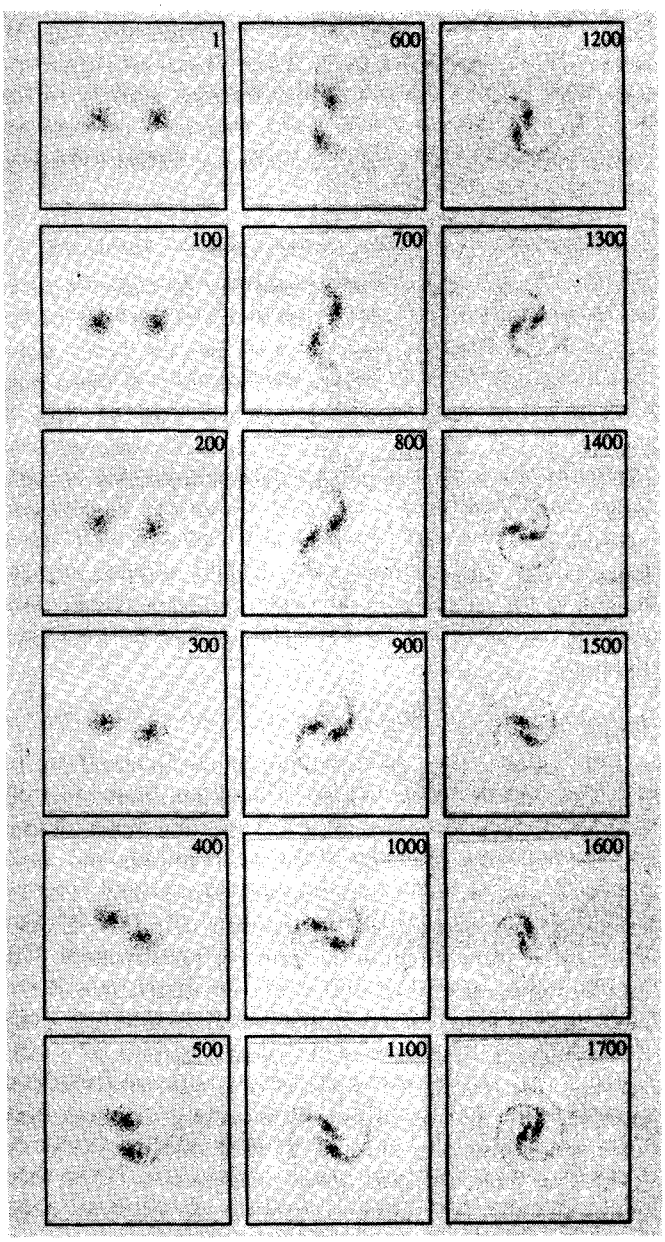

Fig. 6. Single-frame stills of plasma in galaxy simulation run DD4. $\omega_c/\omega_p = 3.0$, $T_{e0} = T_{i0} = 32$ keV, $T = 1$-1700. Acceleration field, 0.0001 cells per time step squared. Not shown is the intergalactic plasma trapped at the geometric center.

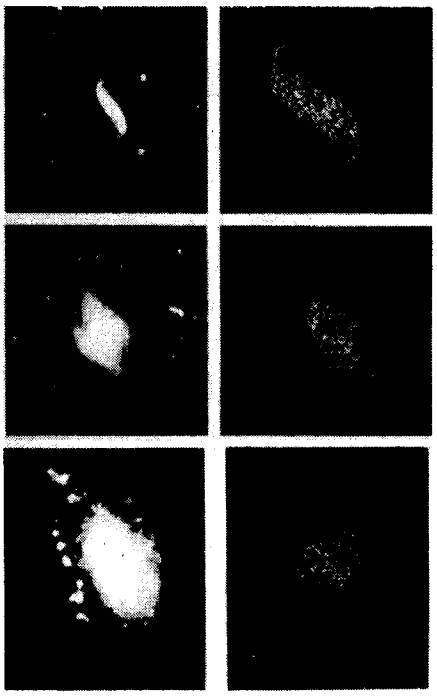

Fig. 7. (a) Selected frames from galaxy simulation run T6D. $\omega_c/\omega_p = 3.0$, $T_{e0} = T_{i0} = 2$ keV. Acceleration field, 0.002 cells per time step squared. (b) Optical photographs of the galaxies NGC 3187, M95, and M64.

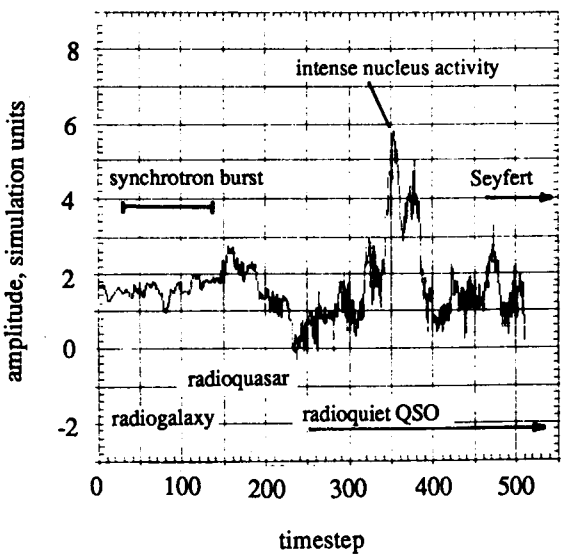

Fig. 8. E_z electric field waveform at center of simulation region for run TD6. Abscissa is given in simulation units (Paper I).

3) a burst of synchrotron radiation from each filament with a total luminosity $L \sim 10^{37}$ W and duration $T \approx 70$–110 [1, fig. 5].

The double radio source with the elliptical plasma at the center and the QSO with the very active nuclear component differ only in the strength of the induction field midway between filament cross sections.

B. Radioquasar to Radioquiet QSO

This phase of the evolution is marked by 1) a decrease in radio lobe (extended component) luminosity when $T >$ 110; and 2) an increase in central component activity for $T \sim$ 250–350. Thus the power in the extended components fades while the increased induction field and the increased compression of plasma in the elliptical sump intensifies the synchrotron radiation from the compact component. The compact component can appear as an isolated synchrotron source during this period (e.g., Fig. 2, linear size ~0.01 kpc).

C. Radioquiet QSO to Seyfert Spiral

The development of the plasma and field morphologies of a radioquiet QSO to a Seyfert spiral actually encompasses a transitional period involving the formation of

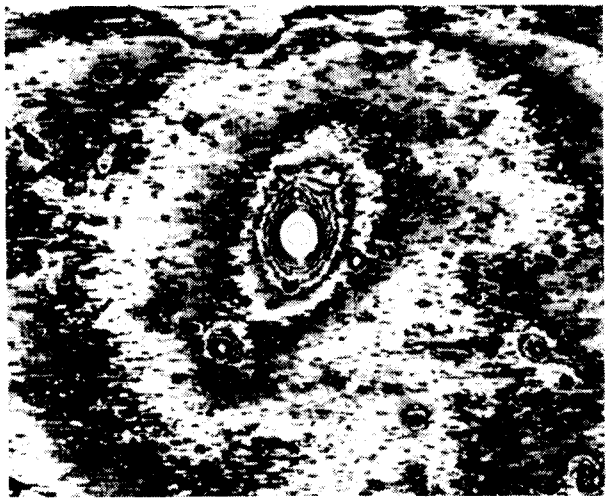

Fig. 9. Isodensitometer tracing of the elliptical galaxy M87, made from a 60-min exposure on IIIa-J emulsion with the 1.2-m Palomar Schmidt telescope. The inner circle is the diameter given in the Shapely-Ames catalogue, while the outer ellipse spans as much as 70 arcmin. The horizontal extent of the image frame is 500 arcmin. Note that the inner isophotes have vertical major axes, but the outer isophotes show noticeable clockwise twisting (cf. [1, Fig. 8]).

several peculiar plasma geometries (Fig. 4, $T \sim 450$–550). (If the ratio of the nucleus luminosity to the luminosity of a galaxy is 0.1 to unity or more, the galaxy is of the Seyfert type.) During this period the incoming plasma of the extended components has not yet coalesced with the quasar center. The synchrotron radio activity in the extended components has decreased markedly (Fig. 8) and the quasar core (≤ 1 kpc) consists of highly activated, strongly radiating, dense ($\sim 10^{10}$ m^{-3}) plasma because of the continued magnetic sump compression ($\sim 10^{-8}$ Pa). The density decreases with isobaric gradient, being tenuous at the periphery of the sump. Time-lapse photography shows that the inward velocities of the isobars are not quite linear in time but pulsate as they compress.

The extended components, quieted for $T > 110$, reappear as the peculiar or spiral plasma morphologies that form about the compact nucleus.

D. Peculiar and Seyfert Galaxies to Spiral Galaxies

Beyond $T \sim 600$, coalescence of the outer plasma components on the excited compact center begins. Additionally, the continued electromagnetic compression on plasma confined in the sump can be expected to start the gravitational collapse of this material. This manifests two effects: the disappearance of the quasar plasma emission and the appearance of stars (Section VIII).

IV. Elliptical Galaxies

Elliptical (E) galaxies, as distinct from peculiars, irregulars, and spirals, are characterized by a very smooth texture, a bright nucleus, and a tenuous outer envelope of large extent (sensitive photographic plates show that the envelope may be 20 times the diameter of the nucleus, Fig. 9) [15]. As mentioned in Section II, Ellipticals are most often found midway between the extended radio components of radio galaxies and radioquasars. Fig. 10 is an example of this geometry. Like S0 galaxies (galaxies with little or no evidence of star-forming activity in the disk) E galaxies are found most frequently in regimes characterized by high galaxy density, i.e., areas most susceptible to *interactions*.

A. Irregular Galaxies and "Dust Lane" E Galaxies

The elliptical sump formed midway between two extended plasma components is the result of the coming together of the magnetic field lines of two (or more) adjacent filaments. At early times, the topology of these field lines is that of two "clashing cymbals" (cf. [1, figs. 6 and 8], that is also the shape taken on by intergalactic plasma between the extended current-conducting components. Examples include not only irregularly shaped galaxies (Fig. 11) but also E and some S0 galaxies with "dust lanes" [12]. The dust lanes are usually aligned perpendicular to the major axis between extended components (Fig. 12), as they must be for plasma pushed in from either filament.

B. Flattened E and S0 Galaxies

Elliptical galaxies are classified in a sequence from E0 to E7, according to the degree of apparent flattening. E0 systems appear circular, and E7 are the most oblong known. All flatter galaxies seem to be spirals and, even among the E7's, many may be type S0, systems that resemble spirals but lack distinctive arms. In fact, E7 galaxies often show slight spiral arms or perturbances. The morphologies described above are the shape that Birkeland currents take when they are closely spaced (e.g., tens of kiloparsecs) or carry weaker galactic currents ($I \sim 10^{17}$ A) (Fig. 13). As shown, when closely adjacent Birkeland currents form out of particle flows along magnetic field lines, a merging and torquing of these plasmas produces forms that have a distinct gap at midsection. These then merge together in rotation to produce an elliptical shape that may exhibit very weak spiral-arm structure.

V. Spiral Galaxies

Hubble originally believed that elliptical galaxies evolve into spiral galaxies [16] and this seems to be borne out by the simulations. However, the simulations show that another class of galaxy, the peculiars [17], [18], bridge the formation of ellipticals to spirals.

Spiral galaxies are the most abundant type known; of all classified galaxies 78 percent are spiral (75 percent normal spiral and 25 percent barred spiral), 18 percent are elliptical, and 4 percent are irregular (Table II).

A. Normal and Barred Spirals

Whether a normal spiral (S) galaxy or a barred spiral (SB) galaxy forms out of the plasma interaction depends primarily on the profile or cross section of the current-carrying filaments, its density distribution, and strength of the azimuthal magnetic fields. Bars form when the interacting plasma regions are sharply divided in plasma

(a)

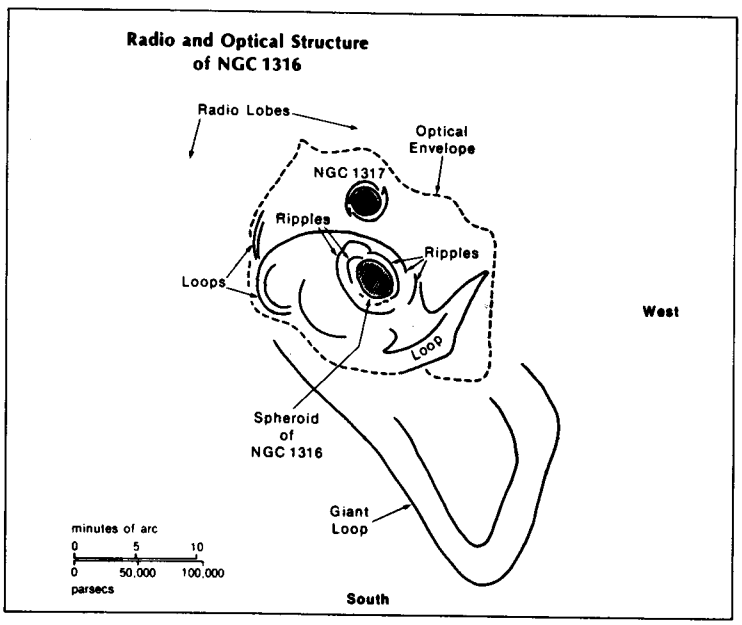

(b)

Fig. 10. (a) Optical photographs of the elliptical galaxy NGC 1316 and the spiral galaxy NGC 1317. (b) Radio and optical structure of NGC 1316 (courtesy of L. Robinson, *Sky Telesc.*, Feb. 1981).

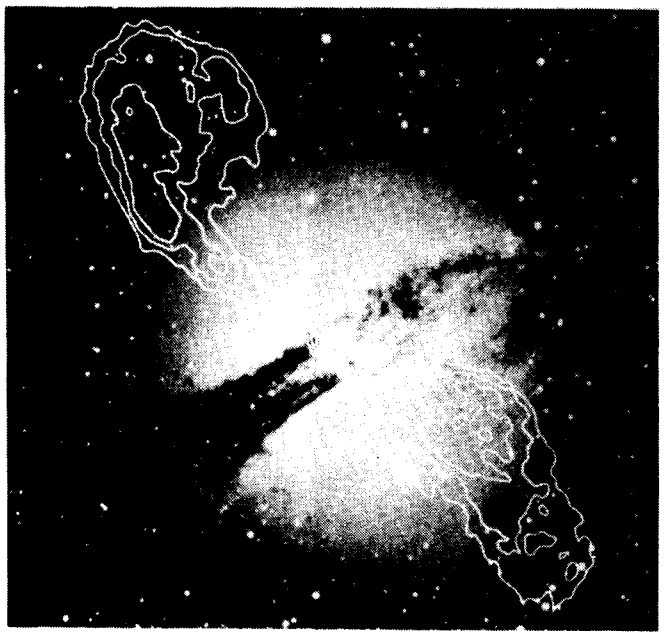

Fig. 11. Radio continuum map of Centaurus A superimposed on an optical photograph from the Hubble atlas (after R. D. Eckers [12]).

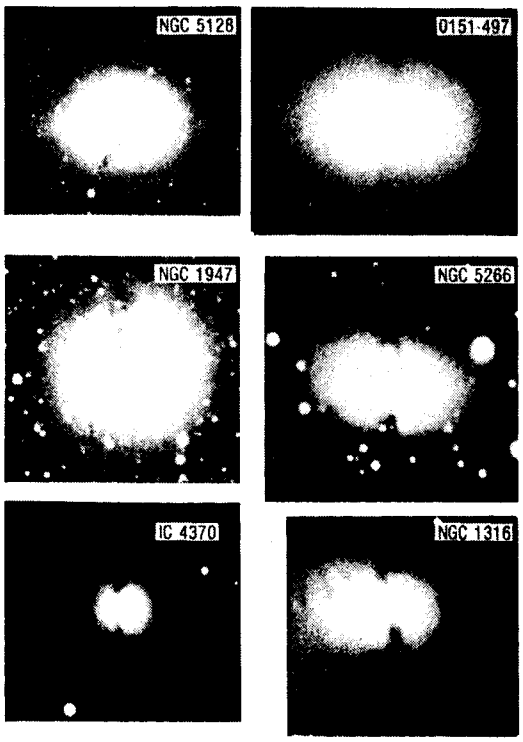

Fig. 12. Optical photographs of "dust-lane" elliptical galaxies NGC 5128, 0151-497, NGC 1947, NGC 5266, IC 4370, and NGC 1316.

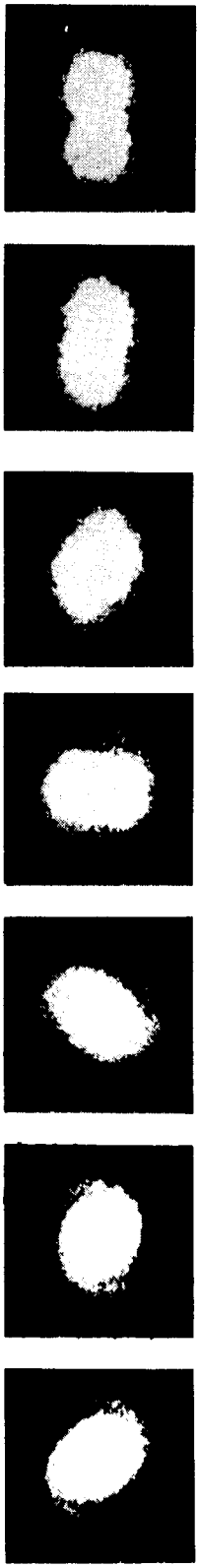

Fig. 13. Single-frame stills of plasma in galaxy simulation D02, $\omega_c/\omega_p = 1.5$.

density, while normal spirals tend to form when the intergalactic plasma supporting the current-conducting filaments is more homogeneous overall.

B. Rotation Characteristics of Spiral Galaxies

Fig. 14 shows the radial velocity versus distance from the galaxy center typical of spiral galaxies [19]–[23]. These data show 1) a nearly linear solid-body rotation for the galaxy center (the first few arcminutes from center); 2) a nearly radially independent velocity profile in the spiral arms; and 3) distinct structure in the spiral arms that appears on the so-called flat portion of the velocity

TABLE II
PERCENTAGE CLASSIFICATION OF OBSERVED AND SIMULATION GALAXIES
(TIME T = 0–2000)

classification	observed	time in classification state, simulated	
Ellipticals	18%	20%	(T=50 to 450)
Irregulars	4%	5%	(T=450 to 550)
Spirals	78%	72.5%	(T=550 to 2000)

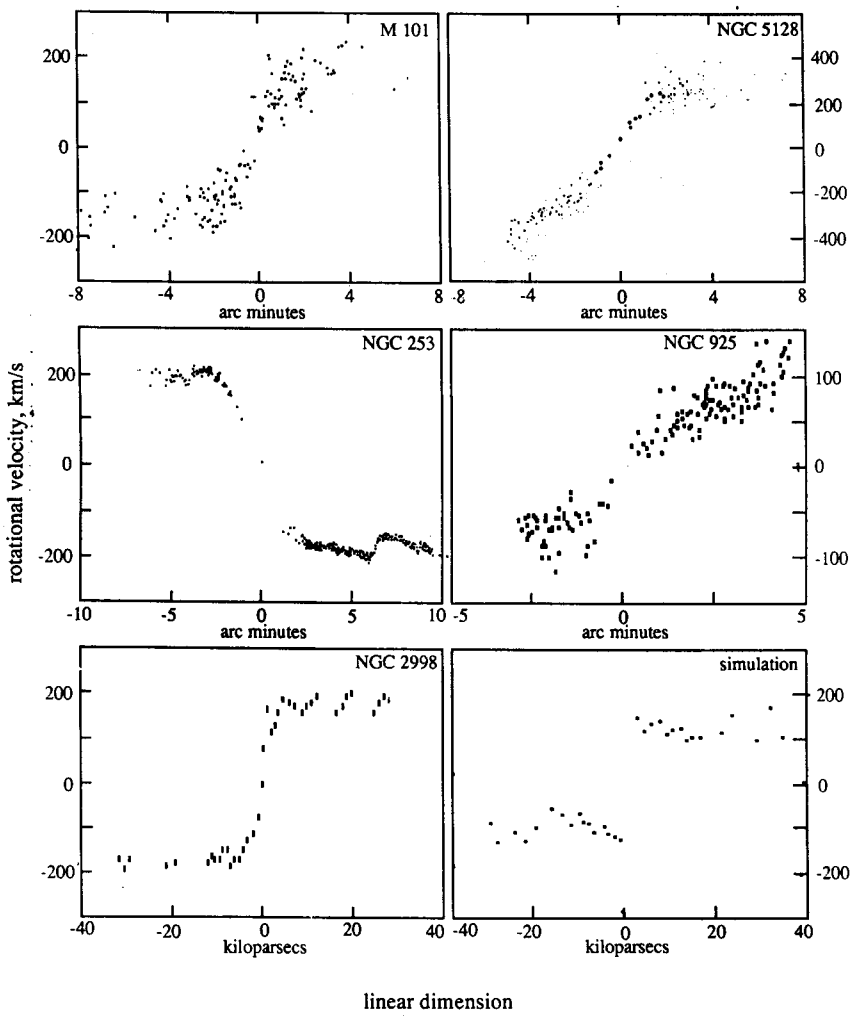

Fig. 14. Spiral galaxy rotational velocity characteristics. The bottom right-hand-side curve is taken from simulation run DD4 during time steps 1745–1746.

curve (beyond the first few arcminutes or, equivalently, the first few kiloparsecs).

The simulated velocity curve in Fig. 14 corresponds to the spiral galaxy in Fig. 6 at time T = 1750 (this curve is the differential rotation measured between T = 1749 and 1750). The simulation data illustrate that 1) the plasma core rotates very nearly as a solid body, and 2) the spirals arms grow in length as they trail out along the magnetic isobars. Concomitant with the lengthening of the arms is a thinning of the arms. Because of this, and the axial current conducted through the thin plasma arms, a diocotron instability is produced. The effect of this instability shows up in both the cross-sectional views of the spiral arms (Figs. 4–7, late time) and in the velocity profile (Fig. 14, simulation curve). Because the plasma in the spiral arms is very nearly neutral (the $\boldsymbol{B} \times \nabla \boldsymbol{B}$ charge separation prevents completely local neutrality), the diocotron instability is moderated somewhat. The azimuthal (sideways) velocity of this instability is given by $V = V' \cot(\psi)$, where V' is the slowly varying radial velocity component and $\psi = \psi(n_e, \boldsymbol{B}, \upsilon_e)$, where υ_e is the effective electron collision frequency in the arm. Good examples of this are found in

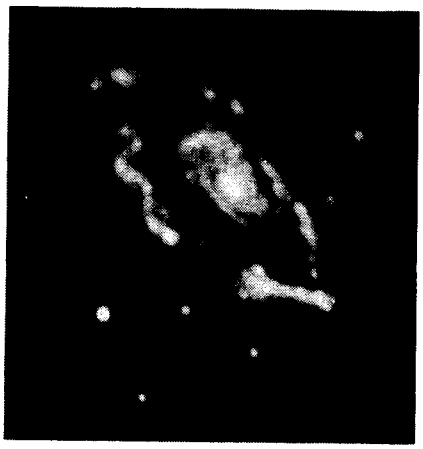

Fig. 15. Optical photographs of the galaxy NGC 3646. Note the well-defined diocotron instability structure in the spiral's arm.

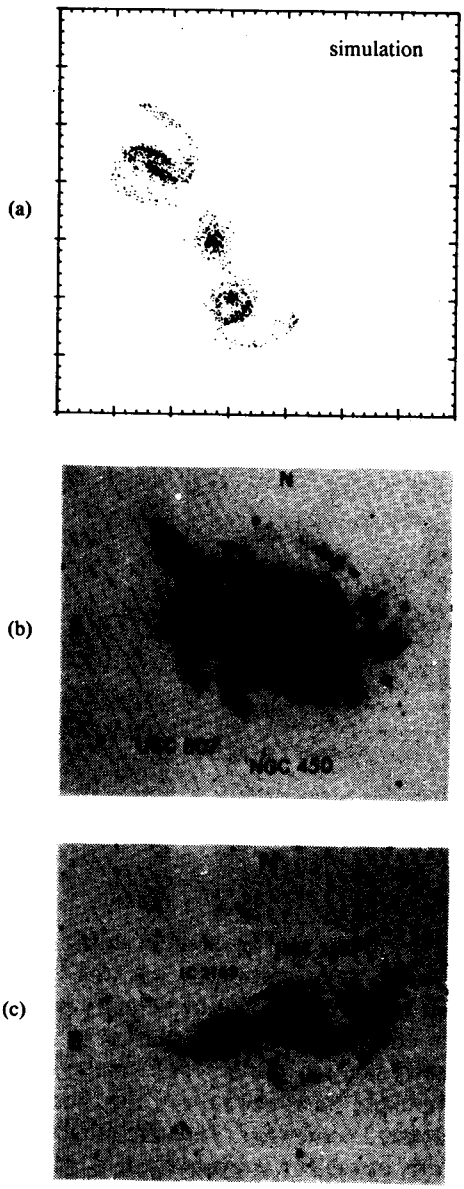

Fig. 16. (a) Single frame from galaxy simulation SAR at $T = 2300$. (b) The interacting pair NGC 450-UGC 807. (c) The interacting galaxy pair IC 2163-NGC 2207.

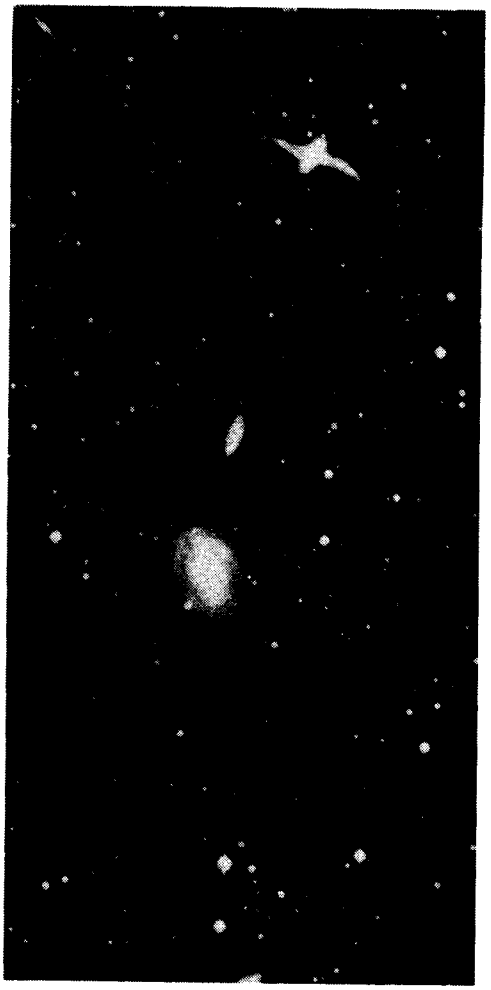

Fig. 17. The Centaurus chain of galaxies. Note that the ring of NGC 4650A (top) is transverse to the chain or filament axis.

the Sc-type galaxies M101, NGC 253, and NGC 2998 (Fig. 14). Fig. 15, NGC 3646, is an example of a very large diocotron instability in the spiral arms.

C. *Evolutionary Sequence for Spiral Galaxies*

It is often the case in the literature that Sa and Sb spirals and Sc and Sd spirals are referred to as "early Hubble types" and "late Hubble types," respectively. However, Hubble emphasized that his classification sequence was not meant to be an evolutionary sequence [16]. The simulations show first the formation of elliptical galaxies. Then, as the synchrotron-radiating Birkeland current-conducting outer plasma components move inward on the elliptical core, peculiar galaxies form and in sequence the spiral types Sd, Sc, Sb, and Sa (or their barred equivalents SBd, SBc, SBb, SBa). Stars form first in the densely compressed elliptical core (Population II stars) and then in the pinched plasma that make up the spiral arms (Population I stars). For Sd and Sc galaxies, the axial Birkeland currents are just reaching the Alfvén–Carlqvist threshold 0.1×10^{-20} A/m^2 (Section VIII) and star formation is irregular. For Sb and Sa galaxies the current is $\geq 10^{-20}$ A/m^2 and star formation follows closely the morphology of the

plasma in the spiral arms that are usually fragmented because of the diocotron instability. The well-known Baade description that stars in spiral arms appear "like beads on a string" is also an equally apropos description for the simulated galaxies. The older elliptical galaxies, compressed in size to make up the core of spiral galaxies, are forced to rotate as a rigid body by the $\boldsymbol{m} \times \boldsymbol{B}$ torques exerted by the incoming outer components while the spiral arms trail behind. The vortex motion of the beads of stars in the arms provides the characteristic $\cot(\psi)$ motion on the rotational velocity curves of spiral galaxies.

VI. Multiple Interacting Galaxies

Birkeland currents often occur in sheets and where these have dimensions of a hundred kiloparsecs or more, filamentation of the plasma into a number of galaxies can take place. Because of the r^{-1} force there is a tendency for filaments to pair up, eventually leading to neighboring spiral galaxies. The classification of multiple interacting galaxies can be spiral–spiral or spiral–peculiar but do not include E or S0 galaxies. Moreover, the spirals tend to be Sd, Sc, or Sb, or the barred equivalents SBd, SBc, or SBb. With this pairing is a decrease in cluster density for the multiply interacting spiral galaxies. Fig. 16(a) shows adjacent spiral galaxies formed from a single sheet Birkeland current. The connection of a spiral configuration to a spherical or oval configuration by a thin filament is a commonly observed morphology, both in simulations and in laboratory experiments [24]. A galactic example of this behavior is the Markarian 205–NCG4319 pair [25]. Fig. 16(b) and (c) shows the interacting spiral pairs IC2163–NGC2207 and UGC807–NGC450 [26]–[29]. Because the Birkeland current is part of a closed-circuit element, galaxies occur periodically along the gigaparsec–subgigaparsec filament where double layers form and where interactions with neighboring filaments occur. The Centaurus chain of galaxies (Fig. 17) may be an example of galaxies forming along filaments.

VII. The Chemical Composition of Forming Galaxies

Cosmic plasma generally is composed of the elements in varying abundances. As such, plasma chemistry plays an important role in the formation of galaxies [30]. The elements in cosmic plasma are detected by absorption and emission lines in the electromagnetic spectrum of cosmic objects.

Neutral hydrogen is detected from galaxies via the Van de Hulst radio-emission line at $\lambda = 21.11$ cm ($f = 1420.4$ MHz), which arises from the transition between the hyperfine-structure sublevels of the ground state of a hydrogen atom [31]. The importance of the study of interstellar hydrogen in this line consists of the fact that this is the sole procedure for direct observation of neutral hydrogen in galaxies.

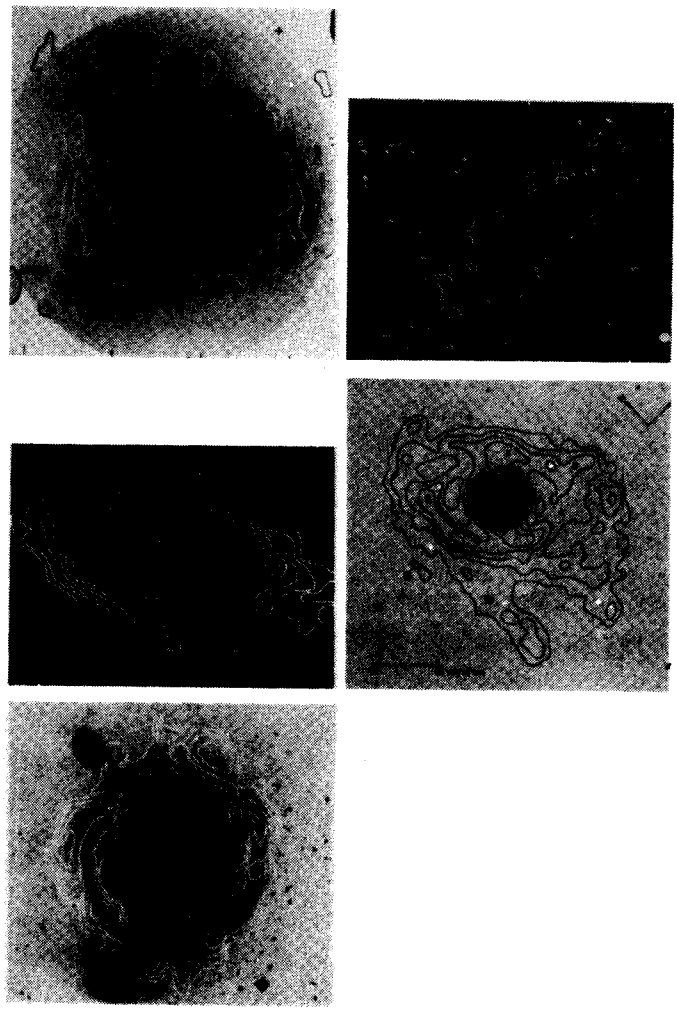

(a) (b)

Fig. 18. HI distributions superimposed on optical photographs of galaxies. (a) NGC 4736 [36], NGC 5033 [37], and NGC 4151 [35]. (b) NGC 3198 [37] and M83 [34].

A. Marklund $\boldsymbol{E} \times \boldsymbol{B}$ Convection and Neutralization of Plasma in Galaxies

Under the influence of the $\boldsymbol{E} \times \boldsymbol{B}$ force, both the electrons and ions drift with the velocity

$$v = (\boldsymbol{E} \times \boldsymbol{B})/B^2 \tag{1}$$

so that the plasma as a whole moves radially inward. This mechanism provides a very efficient convection process for the accumulation of matter from plasma [32]. The material should form as a filamentary structure about the twisted magnetic flux tubes, the lines of which are commonly referred to as "magnetic ropes" because of their qualitative pattern [5]. Magnetic ropes should tend to coincide with material filaments that have a higher density than the surroundings (this is also the case for the filaments in the current sheath of the plasma focus). The cosmic magnetic flux tubes are not directly observable themselves, but the associated filaments of condensed matter can be observed by the radiation they emit and absorb.

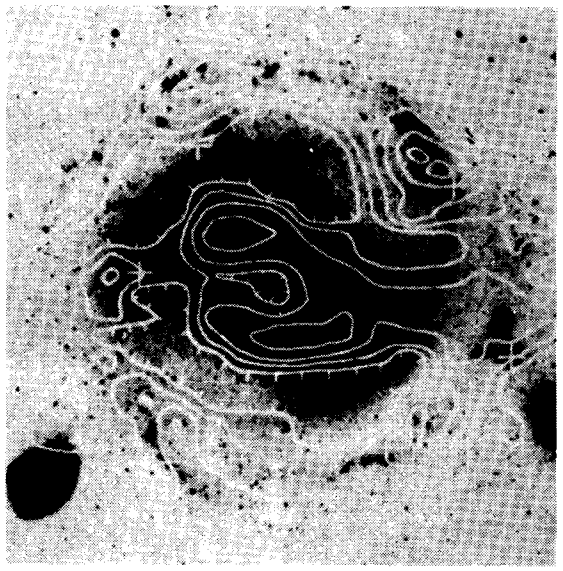

(a)

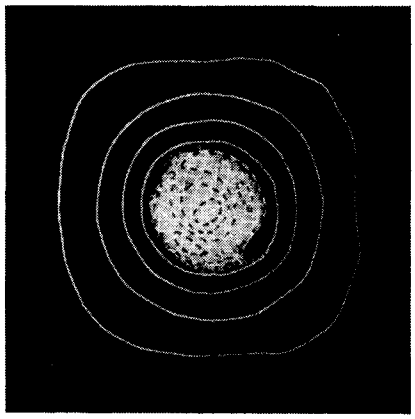

(b)

Fig. 19. (a) HI distribution superimposed on an optical photograph of NGC 4151. (b) Simulation electromagnetic energy density superimposed on simulated plasma galaxy.

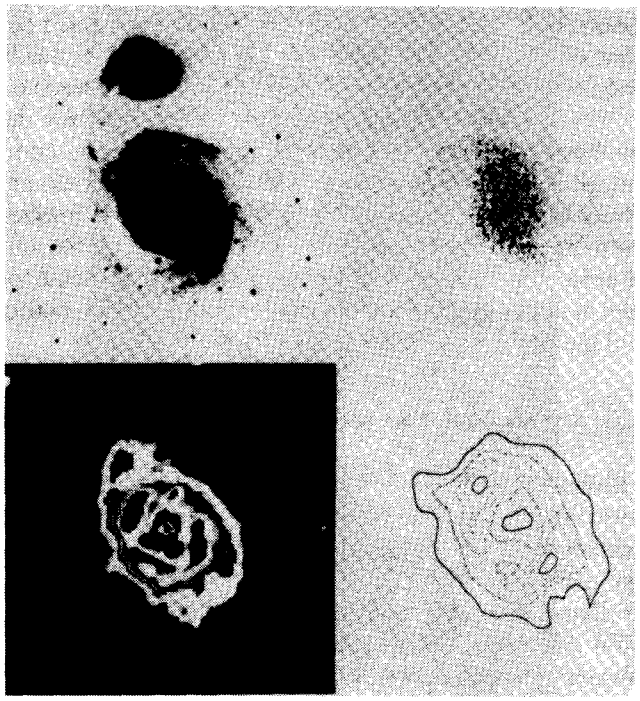

(a) (b)

Fig. 20. (a) Galaxy M51. Top—Infrared photograph, 0.71–0.88-μm, 1.2-m Palomar Schmidt telescope. Bottom—Ultraviolet, 175–275-nm, 0.3-m rocket-borne telescope. (b) Simulation run TO6, time step 600. Top—Plasma distribution. Bottom—Electric (induction) field energy distribution.

Marklund found a stationary state when the inward convection of ions and electrons toward the axis of a filament was matched by recombination and outward diffusion of the neutralized plasma. The equilibrium density of the ionized component normally has a maximum at the axis. However, because of the following mechanism, hollow cylinders, or modifications of hollow cylinders of matter, will form about the flux tubes.

Because of the radiated loss of energy, the filaments cool and a temperature gradient is associated with the plasma. As the radial transport depends on the ionization potential of the element, elements with the lowest ionization potentials are brought closest to axis. The most abundant elements of cosmical plasma can be divided into groups of roughly equal ionization potentials as follows: He(24 eV); H,O,N(13 eV); C,S(11 eV); and Fe,Si,Mg(8 eV). These elements can be expected to form hollow cylinders whose radii increase with ionization potential. Helium will make up the most widely distributed outer layer; hydrogen, oxygen, and nitrogen should form the middle layers; and iron, silicon, and magnesium will make up the inner layers. Interlap between the layers can be expected and, for the case of galaxies, the metal-to-hydrogen ratio should be maximum near center and decrease outwardly. Both the convection process and the luminosity increase with the field E_z.

For the case of a fully ionized hydrogenic plasma, such as that of the simulation model, the ions drift inwards until they reach a radius where the temperature is well below the ionization potential and the rate of recombination of the hydrogen plasma is considerable. Because of this "ion pump" action, hydrogenic plasma will be evacuated from the surroundings and neutral hydrogen will be most heavily deposited in regions of strong magnetic flux [33].

B. Distribution of Neutral Hydrogen in Galaxies

High-resolution observations of neutral hydrogen in irregular and spiral galaxies usually reveal very extended HI distributions. Contour maps of the HI typically show a relative lack of HI in the cores of spiral galaxies but high HI content in the surrounding region, usually in the shape of a "horseshoe" [34]–[40]. This region is not uniform but may have two or more peaks in neutral hydrogen content. Fig. 18 shows several examples of HI distributions in spiral galaxies.

A direct comparison of the simulation predictions is possible by overlaying the simulation galaxy intense B-field distribution (i.e., regions of strong Marklund convection) with the galaxy and also overlaying the HI dis-

tribution of a galaxy with its optical image. Fig. 19 shows the Seyfert NGC 4151 and its simulation analog, while Fig. 20 shows the Seyfert M51 with its simulation analog.

The simulation allows the two peaks in neutral hydrogen to be traced back to their origin. Both are found to be the remnants of the originally extended components, i.e., the original Birkeland filaments. The hydrogen deficient center is the remnant of the elliptical galaxy or quasar core.

VIII. The Alfvén-Carlqvist Model for Star Formation in Pinched Filaments

A. Pinch Compression of Dark Interstellar Clouds

The importance of the pinch effect in interstellar plasma clouds located in galactic-dimensioned current-conducting plasma is illustrated by the following two examples [2].

1) Consider first an interstellar cloud of 100 solar masses, $M_c = 2 \times 10^{32}$ kg, occupying a volume of the linear dimension $l_c = 10^{17}$ m. The temperature of the cloud is $T_c = 10$–10^2 K. This represents a cloud of approximately the same mass as the Orion nebula. The number of atoms present in the cloud is $\sim 10^{59}$, implying a mean density of $n = 10^8$ m^{-3} (10^2 cm^{-3}) and giving $N = 10^{42}$ atoms $\cdot$ m^{-1}. Putting the latter figure and the temperature above into the Bennett relation [1, eq. (4)], we find that an electric current of $I_c \sim 5 \times 10^{13}$–$2 \times 10^{14}$ A has to flow throughout the cloud in order to produce a considerable compressional effect.

2) Consider next a cloud of one solar mass only, $M_c = 2 \times 10^{30}$ kg, having a temperature of $T_c = 10$–10^2 K and an extent of $l_c = 10^{16}$–10^{17} m. Hence, $n = 10^6$–10^9 m^{-3} (1–10^3 cm^{-3}) and $N = 10^{40}$–10^{41} atoms $\cdot$ m^{-1}. The current needed to compress the cloud is now found to be $I_c = 5 \times 10^{12}$–5×10^{13} A.

The current density for both cases outlined above is approximately 0.1–1.0 $\times 10^{-20}$ A/m^2. For the simulated spiral galaxy, $l_c \sim 10$ kpc, $I \sim 10^{20}$ A, so that $j \sim 0.1 \times 10^{-20}$ A/m^2 and the threshold for star formation is met. (Star formation in the elliptical sump is expected to start earlier because of the compressive forces on the dense plasma contained there.)

In the analytical examples above, the interstellar clouds were assumed to be contracted by a Bennett pinch, implying a pure toroidal magnetic field and a pure axial current. According to Alfvén and Carlqvist [2] all magnetic configurations ranging from this kind of pinch to the force-free states would also give rise to contractive forces. For the plasma to pinch in these cases the total current must be larger than that given by the Bennett relation. In order that the total current I_z conducted by the galaxy reach the threshold current density for star formation, it is required that the double layer electric field E_z exist at least to times comparable with the time of spiral formation, i.e., $T \sim 1000$. (The time constant of the gigaparsec length circuit is of order 10^{14} s [1, sec. VIII].)

B. The Motion of Solid Bodies Condensed in Plasma

The motion of a solid particle in a plasma obeys the equation

$$m \frac{dv}{dt} = mg + q(E + v \times B) - \eta v + f \qquad (2)$$

where q is the electric charge of the particle, $-\eta v$ is due to viscosity, and f is the sum of all other forces, including the radiation pressure.

Depending on the size of the particle, we have three typical cases.

1. Very Small Particles: The term $q(E + v \times B)$ dominates over mg and the particle is part of a dusty plasma. Under cosmic conditions this is true if the size of the particle is < 10 nm [30]. In the case of large electric charges the limiting size may rise to 100 nm.

2. Grains: If the size of the particle is so large that the electromagnetic term is negligible, we have an intermediate case dominated by viscosity and gravity. The particles in this regime are referred to as grains. Their equation of motion is

$$\eta v = mg. \qquad (3)$$

Under conditions in interstellar clouds this may be valid for particles of the order of 10 μm.

3. Large Solid Bodies: For "particles" of the size of kilometers or more, the inertia and gravitational terms dominate. Electromagnetic forces are negligible, and viscous forces can be considered as perturbations which may change the orbit slowly. Depending on the properties of the cosmic cloud, viscous forces become important for meter or centimeter sizes. The equation of motion is then

$$m \frac{dv}{dt} = mg - \eta v. \qquad (4)$$

IX. The Extension of Three-Dimensional Electromagnetic Particle Simulations to Include Gravitational Forces

The transition of plasma into stars involves the formation of dusty plasma, the sedimentation of the dust, the formation of stellesimals, and then the collapse into a stellar state. While the above process appears amenable to particle simulation, a crude approximation of proceeding directly from charged particles (actually a cloud of charged particles [1, sec. III]) to mass particles is investigated.

The transition of charge particles to mass particles involves the force constant, that is, the ratio of the coulomb electrostatic force between two charges q separated a distance r

$$F_q(r) = q^2/4\pi\epsilon_0 r^2 \qquad (5)$$

to the gravitational force between two masses m separated a distance r

$$F_G(r) = -Gm^2/r^2. \qquad (6)$$

In the particle algorithm this change is effected by a) changing all particles to a single species; b) limiting the axial extent of the simulation to be of the order of less than the extent or the radial dimension, i.e., about the size of the expected double layer dimension; c) setting the axial velocities to zero; and d) setting the charge-to-mass ratio equal to the negative of the square root of the gravitational constant (times $4\pi\epsilon_0$). This last change produces attractive mass particles via the transformation $\varphi_G(r) = \varphi_q(r)$ in the force equation $\boldsymbol{F} = -\nabla\varphi$, where

$$\varphi_q(r) = q^2/4\pi\epsilon_0 r \tag{7}$$

and

$$\varphi_G(r) = -Gm^2/r \tag{8}$$

are the electrostatic and gravitation potentials, respectively.

Preliminary investigations of the electromagnetic-gravitation potential transformation in three-dimensional codes have been reported elsewhere [41]. The actual process is probably somewhat more complicated than the simplified procedure described above and may involve two interactions: the gravitational force of the plasma arms with stars formed in the arms, and then the gravitational interactions among the stars (themselves gravitationally bound plasmas) in the arms. The earlier formed stars in the elliptical sump plasma must also be included in the simulation. It has been suggested that stars may disperse under gravitational self-forces as the arms rotate, leading to the formation of Sa- and SBa-type galaxies from earlier plasma Sc and Sb and SBc and SBb galaxies [42].

X. Discussion

Between the years 1967 and 1969, excellent reviews and theories on quasars had already appeared that stressed the importance of magnetic fields and plasma theory in order to explain not only the synchrotron radiation observed from quasi-stellar objects but also the morphologies of the extended radio components and the bright cores [43], [44]. These ideas were reexamined by Ginzburg and Ozernoy in a criticism of dense gravitational objects as the source of energy in radio galaxies [45].

The association of an elliptical class of peculiar galaxies with pairs of radio sources has been advocated by Arp [25]–[28]. Arp noted that radio sources with similar flux densities tend to form pairs separated 2°–6° on the sky and stated there was a tendency for a certain class of peculiar galaxy to fall approximately on the line joining the pair. These peculiar galaxies are often elliptical galaxies that show evidence for structures that may have been ejected from (or are falling into) them [46], [47].

The simulations show that, depending on the time of evolution, both processes occur. At early time, the compression of intergalactic plasma in the sump produces the peculiar elliptical-like morphologies observed (Section IV-A and Fig. 9). At yet later time, the "ejection" of plasma on a line connecting two extended radio components is caused by a reconfiguration of the magnetic isobars so that first plasmoids, then flattened "jets" appear on either side of the elliptical sump. (These geometries are formed as the isobaric profiles act on the confined plasma.) The flattened magnetic field minima on either side of the sump produce a plasma trap so that quasars tend to form along this line. Spiral arms form as the outer plasmas from the extended radio components move inward and rotate around, and then coalesce with the elliptical center.

XI. Conclusion

The difficulties encountered in explaining the dynamics of elliptical and spiral galaxies in the absence of magnetic fields and plasma physics are well known [15], [48]. In a very perceptive paper, Toomre [49] questions the dilemma that photographic data of galactic mergers present to gravitational N-body simulations. The complexity of this problem is further compounded by the existence of peculiar galaxies, the morphologies and topologies of which do not inspire confidence in theories postulating linear waves or shocks as the molding forces [50]–[52]. Observationally, these difficulties are perhaps best summarized in *The Atlas of Peculiar Galaxies* [18].

> The *Atlas* as it has been realized in the following pages illustrates again that galaxies cannot be characterized as just assemblages of stars, radiation, and gravitation. The following *Atlas* pictures emphasize the importance of dust in some; they particularly imply a much more important role for the gas in general and point to the existence of either new forces or forces which previously have been little considered. For example, the twisted distorted shapes and curious linkages pictured here attest to the fact that there are viscosity-like forces present that in some cases are dominant. Probably these forces are due to magnetic effects. Vorontsov-Velyaminov has stressed in the past the probable magnetic nature of these effects. Magnetic forces are very difficult to study, but may be very important in our Universe. The recent radio-astronomy discoveries of violent events in galaxies reveal sources of energetic charged particles. These charged particles interact with magnetic fields and offer the hope of mapping, measuring, and understanding cosmic magnetic fields. Exploration of the connection between the plasmas observed with the radio telescopes and the optical evidences of plasma effects pictured in the present *Atlas* is now open to us.

This paper and its predecessor (Paper I) have addressed the evolution of the plasma universe in order to understand both electromagnetic spectra over ten octaves, as well as the visual morphologies observed at optical wavelengths.

It is emphasized that the simulations described in Papers I and II do not pertain to wandering plasma clouds or galaxies whose happenchance encounters might be

thought to produce tails or spiral structure. In a universe of plasma, Birkeland current sheets (i.e., the flow of charged particles along magnetic field lines) can occur wherever a circuit and potential source exist. The source can simply be the transverse motion of plasma of dimension 10–50 Mpc through a 10^{-9}-T field at ~ 1000 km/s. The circuit is thought to be composed of plasma whose filamental length, in analogy to laboratory filaments, may be hundreds of megaparsecs. As in the laboratory, Birkeland current sheet filaments, and lumps within the filaments interact with their neighbors to produce the phenomena outlined in this paper.

Two plasma columns, as modeled here, represent the two closest filaments in a Birkeland sheet (Fig. 16 is a simulation where the initial plasma configuration was a Birkeland sheet). When the plasma profile, density, temperature, strength, and orientation of any external fields have been specified, no additional assumptions are possible in a simulation; the configuration will evolve through cascades of nonlinear states according to the electromagnetic (and when present, gravitational) forces on the plasma. In this regard, the data presented here were obtained by postprocessing the simulation particle, field, probe, and history dumps. The totally unexpected (to the author) phenomena replicated in the simulations appear to be far more universal than the interacting laboratory z pinches for which they were intended. When scaled to cosmic dimensions the simulations show:

1) a burst of synchrotron radiation of luminosity $\sim 10^{37}$ W lasting 10^7–10^8 years as the interaction began;
2) isophotal topologies of double radio galaxies and quasars, including juxtapositioned "hot spots" in the radio lobes (cross sections of the interacting Birkeland currents);
3) the formation of "dust lane" peculiar and elliptical galaxies at the geometric center of quasars and radio galaxies (due to plasma trapped and compressed within the elliptical magnetic separatrix);
4) a spatially varying power law along the major axis of the simulated double radio galaxies in agreement with observations;
5) alternating beams of betatron-pumped synchrotron-emitting electrons on either side of the elliptical center (these have the morphologies (i.e., "knots" or vortices) and polarization properties of jets); and
6) a "superluminosity" and fading of jets as the betatron-induced acceleration field sweeps over and ignites previously confined plasma.

The simulation time frame of this investigation lasted some 10^8–10^9 years. The lifetime and evolution of quasars and double radio sources, the so-called end problem of double radio galaxies, was addressed in this paper (Paper II) by continuing the simulation run ~ 1–5×10^9 years farther in time. This extension of the simulation showed:

1) the transition of double radio galaxies to radioquasars to radioquiet QSO's to peculiar and Seyfert galaxies, finally ending in spiral galaxies;
2) the formation of irregular and dust lane galaxies, as well as more flattened E and S0 galaxies within the magnetic separatrix;
3) barred and normal spiral galaxies resulting from the inflow of plasma from the outer Birkeland currents onto the the elliptical galactic center; the characteristic rotational velocities of spiral galaxies including the fine-detail vortex cotangent structure on the "flat" portions of the spiral-arm velocity components;
4) replications of the morphologies of multiple interacting galaxies;
5) "horseshoe" like regions of nearly neutral HI gas in spiral galaxies resulting from the convection and neutralization of plasma into regions of strong galactic magnetic fields; and
6) toroidal and poloidal components of the galactic magnetic field with field strengths reaching 2×10^{-4} G at the galactic center (fields as high as 10^{-2} G can occur in concentrated regions). These results were reported prior to their observation in the Galaxy [41].

Finally, the pinch effect from the currents carried in the galactic plasmas illustrates the importance of the electromagnetic field in initiating the first stages of dusty plasma collapse into stellisimals, then into stars [53].

The investigation of complex filamentation processes in laboratory plasmas by the particle-in-cell approach has thus led to unexpected analogies in cosmic plasmas. As computer powers (i.e., speed and memory) increase, the ability to resolve and understand the evolution of the plasma universe in greater detail can be expected. Perhaps as important, as the universe represents an unprecedented plasma data bank, insights on laboratory data can also be expected.

REFERENCES

[1] A. L. Peratt, "Evolution of the plasma universe: I. Double radio galaxies, quasars, and extragalactic jets," *IEEE Trans. Plasma Sci.*, vol. PS-14, no. 6, pp. 639–660, Dec. 1986.
[2] H. Alfvén and P. Carlqvist, "Interstellar clouds and the formation of stars," *Astrophys. Space Sci.*, vol. 55, pp. 484–509, 1978.
[3] R. Beck, "Magnetic fields and spiral structure," in *Internal Kinematics and Dynamics of Galaxies*, E. Athanassoula, Ed. Amer. Astron. Union, 1983, pp. 159–160.
[4] R. Beck, "Interstellar magnetic fields," *IEEE Trans. Plasma Sci.*, vol. PS-14, no. 6, pp. 740–747, Dec. 1986.
[5] H. Alfvén, *Cosmic Plasma*. Dordrecht, Holland: Reidel, 1981.
[6] H. Alfvén, "Paradigm transition in cosmic plasma physics," *Physica. Scripta*, vol. T2/1, pp. 10–19, 1982.
[7] H. Alfvén, "Double layers and circuits in astrophysics," *IEEE Trans. Plasma Sci.*, vol. PS-14, no. 6, pp. 779–793, Dec. 1986.
[8] H. Alfvén and D. A. Mendis, "Plasma effects in the formation, evolution and present configuration of the Saturnian ring system," *Adv. Space Res.*, vol. 3, pp. 95–104, 1983.
[9] G. Burbidge and M. Burbidge, *Quasi-Stellar Objects*. San Francisco, CA: Freeman, 1967, pp. 85–94.
[10] R. Fanti and G. C. Perola, in *Radio Astronomy and Cosmology*, D. L. Jauncy, Ed. (IAU Symp. 74). Dordrecht, Holland: Reidel, 1977, p. 171.
[11] G. C. Perola, "Radio galaxies: Observations and theories of their extended components," *Fundamentals of Cosmic Phys.*, vol. 7, pp. 59–130, 1981.
[12] R. D. Ekers, "Radio observations of the nuclei of galaxies," in *The*

Formation and Dynamics of Galaxies, J. R. Shakeshaft, Ed. (IAU Symp. 58). 1974, pp. 257-277.
[13] W. H. Bostick, "Simulation of astrophysical processes in the laboratory," *Nature*, vol. 173, p. 214, 1957.
[14] W. H. Bostick, "Experimental study of plasmoids," in *Electromagnetic Phenomena in Cosmical Physics*, B. Lehnert, Ed. (Int. Astron. Union Symp. 6, Stockholm, Sweden, 1956). Cambridge, England: Cambridge, 1958, pp. 87-98.
[15] K. M. Strom and S. E. Strom, "Galactic evolution: A survey of recent progress," *Science*, vol. 216, pp. 571-580, 1982.
[16] E. Hubble, *The Realm of the Nebulae*. New York: Dover, 1958.
[17] B. A. Vorontsov-Velyaminov, *Atlas and Catalogue of Interacting Galaxies*, vol. 1. Moscow, USSR: Sternberg Inst., Moscow State Univ., Moscow, 1959.
[18] H. Arp, *Atlas of Peculiar Galaxies* (*Astrophys. J.* Supplement series 123-132), vol. 14, 1966, pp. 1-57.
[19] V: C. Rubin, W. K. Ford, Jr., and N. Thonnard, "Extended rotation curves of high-luminosity spiral galaxies. IV. Systematic dynamical properties, Sa-Sc," *Astrophys. J.*, vol. 225, pp. L107-L111, 1978.
[20] G. deVaucouleurs, "Surveying velocity fields in galaxies," *Sky Telesc.*, vol. 62, pp. 406-410, 1981.
[21] M. Marcelin, J. Boulesteix, and G. Courtés, "The velocity field of the ionized gas in the barred galaxy NGC 925," *Astron. Astrophys.*, vol. 108, pp. 124-140, 1982.
[22] M. Marcelin, J. Boulesteix, G. Courtes, and B. Milliard, "NGC 5128—A galaxy with a recently formed disk," *Nature*, vol. 297, pp. 38-42, 1982.
[23] R. Louise and M. Marcelin, "Mass model of spiral galaxies disk," *Astrophys. Space Sci.*, vol. 91, pp. 93-98, 1983.
[24] H. F. Webster and T. S. Hallinan, "Instabilities in charge sheets and current sheets and their possible occurrence in the aurora," *Radio Sci.*, vol. 8, pp. 475-482, 1973.
[25] J. W. Sulentic, "Confirmation of the luminous connection between NGC 4319 and Markarian 205," *Astrophys. J. Lett.*, vol. 265, pp. L49-L53, 1983.
[26] H. Arp. "Three new cases of galaxies with large discrepant redshifts," *Astrophys. J.*, vol. 239, pp. 469-474, 1980.
[27] H. Arp, "Characteristics of companion galaxies," *Astrophys. J.*, vol. 256, pp. 54-74, 1982.
[28] H. Arp, "Further examples of companion galaxies with discordant redshifts and their spectral peculiarities," *Astrophys. J.*, vol. 263, pp. 54-72, 1982.
[29] H. Arp, "Further observations and analysis of quasars near companion galaxies," *Astrophys. J.*, vol. 271, pp. 479-506, 1983.
[30] H. Alfvén and G. Arrhenius, *Evolution of the Solar System*. Washington, DC: NASA, 1976, SP-345.
[31] S. A. Kaplan and S. B. Pikelner, *The Interstellar Medium*. Cambridge, MA: Harvard Univ. Press, 1970.
[32] G. T. Marklund, "Plasma convection in force-free magnetic fields as a mechanism for chemical separation in cosmical plasmas," *Nature*, vol. 277, pp. 370-371, 1979.
[33] I. F. Mirabel and R. Morras, "Evidence for high-velocity inflow of neutral hydrogen toward the galaxy," *Astrophys. J.*, vol. 279, pp. 86-92, 1984.
[34] D. H. Rogstad, I. A. Lockhart, and M. C. H. Wright, "Aperture-synthesis observations of the HI in the galaxy M85," *Astrophys. J.*, vol. 193, pp. 309-319, 1974.
[35] A. Bosma, R. D. Ekers, and J. Lequeux, "A 21-cm study of the Seyfert galaxy NGC 4151," *Astron. Astrophys.*, vol. 57, pp. 97-104, 1977.
[36] A. Bosma, J. M. Van de Hulst, and W. T. Sullivan III, "A neutral hydrogen study of the spiral galaxy NGC 4736," *Astron. Astrophys.*, vol. 57, pp. 373-381, 1977.
[37] A. Bosma, "21-cm line studies of spiral galaxies. I. Observations of the galaxies NGC 5033, 3198, 5055, 2841, and 7331," *Astron. J.*, vol. 86, pp. 1791-1824, 1981.
[38] A. Bosma, "21-cm line studies of spiral galaxies. II. The distribution and kinematics of neutral hydrogen in spiral galaxies of various morphological type," *Astron. J.*, vol. 86, pp. 1825-1846, 1981.
[39] E. Hummel and A. Bosma, "Radio continuum observations of the spiral galaxies NGC 2841, NGC 5055, and NGC 7331," *Astron. J.*, vol. 87, pp. 242-251, 1982.
[40] H. Van Woerden, W. Van Driel, and U. J. Schwarz, "Distribution and motions of atomic hydrogen in lenticular galaxies," in *Internal Kinematics and Dynamics of Galaxies*, E. Athanassoula, Ed. Amer. Astron. Union, 1983, pp. 99-104.
[41] A. L. Peratt, "Simulating spiral galaxies," *Sky Telesc.*, vol. 68, pp. 118-122, 1984.
[42] E. J. Lerner, private communication, 1986.
E. J. Lerner, "Magnetic self-compression in laboratory plasmas, quasars and radio galaxies," *Lasers and Particle Beams*, vol. 4, part 2, pp. 193-222, 1986.
[43] H. J. Smith, "Observed characteristics of quasars," in *Quasars and High Energy Astronomy*, K. N. Douglas *et al.*, Eds. New York: Gordon and Breach, 1969, pp. 167-180.
[44] P. A. Sturrock, "Explosions in galaxies and quasars," in *Plasma Instabilities in Astrophysics*, D. G. Wentzel and D. A. Tidman, Eds. New York: Gordon and Breach, 1969, pp. 297-328.
[45] V. L. Ginzburg and L. M. Ozerney, "On the nature of quasars and active galactic nuclei," *Astrophys. Space Sci.*, vol. 50, pp. 23-41, 1977.
[46] H. Arp, "Peculiar galaxies and radio sources," *Astrophys. J.*, vol. 148, pp. 321-365, 1967.
[47] H. Arp, "Ejection from galaxies and galaxy formation," in *Problems of Physics and Evolution of the Universe*, L. V. Mirzoyan, Ed. Erevan, Armenia: Armenian Acad. of Sci., 1978, pp. 65-96.
[48] A. Toomre, "Theories of spiral structure," *Annu. Rev. Astron. Astrophys.*, vol. 15, pp. 437-478, 1977.
[49] A. Toomre, "Mergers and some consequences," in *The Evolution of Galaxies and Stellar Populations*, B. M. Tinsley and R. B. Larson, Eds. New Haven, CT: Yale Univ. Observatory, 1977, pp. 401-426.
[50] H. Arp, "The persistent problem of spiral galaxies," *IEEE Trans. Plasma Sci.*, vol. PS-14, no. 6, pp. 748-762, Dec. 1986.
[51] J. H. Piddington, "The density-wave theory of galactic spirals," *Astrophys. J.*, vol. 179, pp. 755-770, 1973.
[52] J. H. Piddington, "The role of magnetic fields in extragalactic astronomy," *Astrophys. Space Sci.*, vol. 80, pp. 457-471, 1981.
[53] B. E. Meierovich, "Electromagnetic collapse, problems of stability, emission of radiation and evolution of a dense pinch," *Phys. Reports*, vol. 104, pp. 259-347, 1984.